Journal of the Korean Physical Society, Vol. 55, No. 2, August 2009, pp. 675∼680

Impact of the Parameters for a Chemically-amplified Resist on the Line-edge-roughness by Using a Molecular-scale Lithography Simulation

Sang-Kon Kim,* Hye-Keun Oh, Young-Dae Jung and Ilsin An
Department of Applied Physics, Hanyang University, Ansan 426-791

(Received 23 March 2009)

Resists require higher resolution, lower line-edge roughness (LER) (or line-width roughness (LWR)), and improved sensitivity. However, those characteristics have an uncertain triangular relation and require trade-off. In this paper, a molecular-scale Monte Carlo simulation of the master equations is described. The master equations are proven analytically to be the rate equations of the chemically-amplified resist (CAR). The impact of various parameters, the aerial image contrast, the photoacid generator, the acid diffusion length, the quencher, the acid, the quencher diffusion coefficients, and the polymer size, on the LER in a CAR is analyzed with the Taguchi method and the spatial scaling metrics of CAR-induced LER. Simulation results for the 3σ LER agree with the experimental results, so a molecular-scale simulator can predict the dependence of the LER on the material properties and the process conditions. The HHCF (Height-height correction function) of spatial scaling metrics for the resist characterization and the Taguchi method for the LER minimization are discussed.

PACS numbers: 85.40.HP, 78.20.Bh, 81.16.Nd, 82.20.Wt
Keywords: Lithography, Lithography simulation, Monte-Carlo, Molecular, Molecular-scale simulation, Taguchi method, Line-edge roughness, Chemically-amplified resist

I. INTRODUCTION

According to the international technology roadmap for semiconductor (ITRS), the line-edge roughness (LER) can be controlled at below 1.2-nm for the 22-nm pattern formation. However, the triangular relation between the resolution, LER, and sensitivity is uncertain. During the post exposure bake (PEB) process, the fluctuations of the number of inhibitor groups and the correlations among the different particle numbers cannot be taken into account with the standard rate equation approach. For shot noise and lithographically interesting structure sizes of a few tens of nanometers, the standard approach cannot offer the advantage of modeling statistical printing defects. Hence, for the analysis of process and resist material factors in the below 22-nm pattern formation, a molecular-scale simulation is required. The Monte Carlo method deals with length scales between the atomistic scale and the continuum model scale. The essential idea of the Monte Carlo method is not to evaluate the photo- and thermal-chemical reaction at every component of a chemically-amplified resist (CAR), but rather at only a representative random sampling of abscissae. Schmid *et al.* described the molecular level effects as acid distribution for the PEB and as the resist feature roughness for development by using the Monte Carlo method [1]. Mülders *et al.* used the Markov processes with the Monte Carlo method to model the kinetics of the chemical reactions of the PEB and development [2]. However, a simple and practical algorithm and an analysis of molecular-scale simulation have been of interest for understanding complex molecular phenomenon.

In this paper, a molecular-scale simulation based on the Monte Carlo method and the master equation are described. For its results, the impacts of the resist components on the LER are analyzed by using the Taguchi method and the spatial scaling metrics of the CAR-induced LER.

II. MONTE CARLO SIMULATION FOR PEB

When CAR is exposed to light, acid is generated by conversion of the photo-acid generator (PAG). During the PEB, this initial acid derives the de-protection reaction with the thermal-acid-catalyzed reaction, which alters the development rate of the resist. The master equation of the Monte-Carlo process for the PEB can be viewed as a gain-loss balance:

$$\frac{dP\left(n_M,n_H,n_Q,t\right)}{dt}=\tau^{+}\left(n_M,n_H,n_Q,t\right) -\tau^{-}\left(n_M,n_H,n_Q,t\right), \quad (1)$$

*E-mail: sangkona@hotmail.com; http://www.sangkon.info

where P is the probability, n_H is the number of acid molecules, n_Q is the number of quencher molecules, and n_M is the number of blocked polymer sites. τ^+ is the probability that some other state will be converted into the state with (n_M, n_H, n_Q) molecules. τ^- is the probability that the state with (n_M, n_H, n_Q) molecules will be converted into some other state either by a deblocking reaction or by acid-base quenching. The functions (τ^+ and τ^-) as transition probabilities can represent, respectively,

$$\begin{aligned}
&\tau^+ (n_M, n_H, n_Q, t) \\
&\quad = k_1 n_H (n_M + 1) P (n_H, n_Q, n_M + 1) \\
&\quad + k_2 (n_H + 1) P (n_M, n_H + 1, n_Q) \\
&\quad + k_3 (n_H + 1) (n_Q + 1) P (n_M, n_H + 1, n_Q + 1), \quad (2) \\
&\tau^- (n_M, n_H, n_Q, t) = k_1 n_H n_M P (n_M, n_Q, n_M) \\
&\quad + k_2 n_H P (n_M, n_H + 1, n_Q) \\
&\quad + k_3 n_H n_Q P (n_M, n_H + 1, n_Q + 1). \quad (3)
\end{aligned}$$

The time derivative of the average number of blocked polymer sites in Eq. (1) can be written as

$$\begin{aligned}
\frac{\langle n_M \rangle}{dt} &= k_1 \sum_{n_M, n_H, n_Q} \{(n_M - 1) n_M n_H P \\
&\quad \times (n_M + 1, n_H, n_Q) - n_M^2 n_H P (n_M, n_H, n_Q)\} \\
&\quad + k_2 \sum_{n_M, n_H, n_Q} \{n_M n_H P (n_M, n_H + 1, n_Q) \\
&\quad - n_M n_H P (n_M, n_H, n_Q)\} \\
&\quad + k_3 \sum_{n_M, n_H, n_Q} \{n_M n_H n_Q P (n_M, n_H, n_Q) \\
&\quad - n_M n_H n_Q P (n_M, n_H, n_Q)\} \quad (4) \\
&= -k_1 \langle n_M, n_H \rangle = -k_1 [\langle n_M \rangle \langle n_H \rangle + \alpha (n_M, n_H)],
\end{aligned}$$

where k_1 is the acid-catalyzed deprotection rate, $\alpha (n_M, n_H)$ is $\langle n_M, n_H \rangle - \langle n_M \rangle \langle n_H \rangle$, $\langle n_M \rangle = \sum_{n_M, n_H, n_Q} n_M P (n_M, n_H, n_Q)$, and $\langle n_H \rangle = \sum_{n_M, n_H, n_Q} n_H P (n_M, n_H, n_Q)$. Eq. (4) is corresponds to the rate equation $d [M] / dt = -k_{amp} \cdot [M] \cdot [A]^m$, which means that the photo-generated acid catalyzes a thermally-induced reaction that cleaves the protecting groups and renders the reacted (deprotected) region (X_M) soluble in an aqueous developer (M + A $\rightarrow$ X_M + A, where A is acid and M is protecting group). According to Eq. (4), the time derivative of the average number of acid molecules is

$$\frac{d\langle n_H \rangle}{dt} = -k_2 \langle n_H \rangle - k_3 [\langle n_H \rangle \langle n_B \rangle + \alpha (n_H, n_B)], \quad (5)$$

where k_2 is the acid loss reaction rate and k_3 is the acid neutralization rate. Eq. (5) corresponds to the rate equation $d [A] / dt = -k_{loss} \cdot [A] - k_{quench} \cdot [A] \cdot [B] + \nabla \cdot (D_{acid} \nabla [A])$, which means that acid is loss (A $\rightarrow \oslash$, where $\oslash$ is empty) and diffuses from a high-dose region to a low-dose region, washing out standing waves and causing the reacted region to be larger than the initially exposed region. According to Eq. (4), the time derivative of the average number of quencher molecule is

$$\frac{d\langle n_Q \rangle}{dt} = -k_3 [\langle n_H \rangle \langle n_B \rangle + c (n_H, n_B)], \quad (6)$$

where k_3 is the acid neutralization rate and $\langle n_Q \rangle = \sum_{n_M, n_H, n_Q} n_Q P (n_M, n_H, n_Q)$. Eq. (6) corresponds to the rate equation $d [B] / dt = -k_{quench} \cdot [A] \cdot [B]$, which means that the quencher neutralizes the acid (A + B $\rightarrow X_{AB}$, where B is the quencher and X_{AB} is acid neutralization) [3].

III. TAGUCHI METHOD

The Taguchi method is a powerful method for the integration of design of experiments (DOE) with parametric optimization of the process, yielding the desired results by using an orthogonal array experiments that provide much-reduced variance for the experiments. Hence, this method is a simple and efficient method to find the best range of designs for quality, performance, and computational cost by using a statistical measure of performance called the signal-to-noise ratio (S/N). The S/N ratio is defined as the ratio of the mean (signal) to the standard deviation (noise). The kinds of S/N ratios are lower-the-better (LB), higher-the-better (HB), and nominal-the best (NB). The S/N ratio for LER is the LB (lower-the-better) criterion, which is

$$S/N = -10 \log \left(\frac{1}{n} \sum y^2 \right), \quad (7)$$

where y is the observed data and n is the number of observations. The parameter level combination that maximizes the appropriate S/N ratio is the optimal setting [4].

IV. SIMULATION RESULTS AND ANALYSIS

Figure 1 shows Monte Carlo simulation results of lithography processes for the two-dimensional plane (100 nm × 100 nm) of a molecular resist. The initial quantities of acid, quencher, inhibitor, and PAG are generated among the cells by randomly distributing a user-defined number of each molecule. The resist is a mixed distribution of acid (5.04%) with a 2-nm diffusion length (DL) coefficient, PAG (10.48%), quencher (5.4%) with a 2-nm DL coefficient, and inhibitors (5.4%) in Fig. 1(e). The two-dimensional aerial image deposited onto the surface of a simulated film is calculated by using a homemade tool based on the rate equations [5]. The illumination conditions are a 193-nm wavelength, polarization dipole illumination with a 45° opening angle, a 0.5-μm offset,

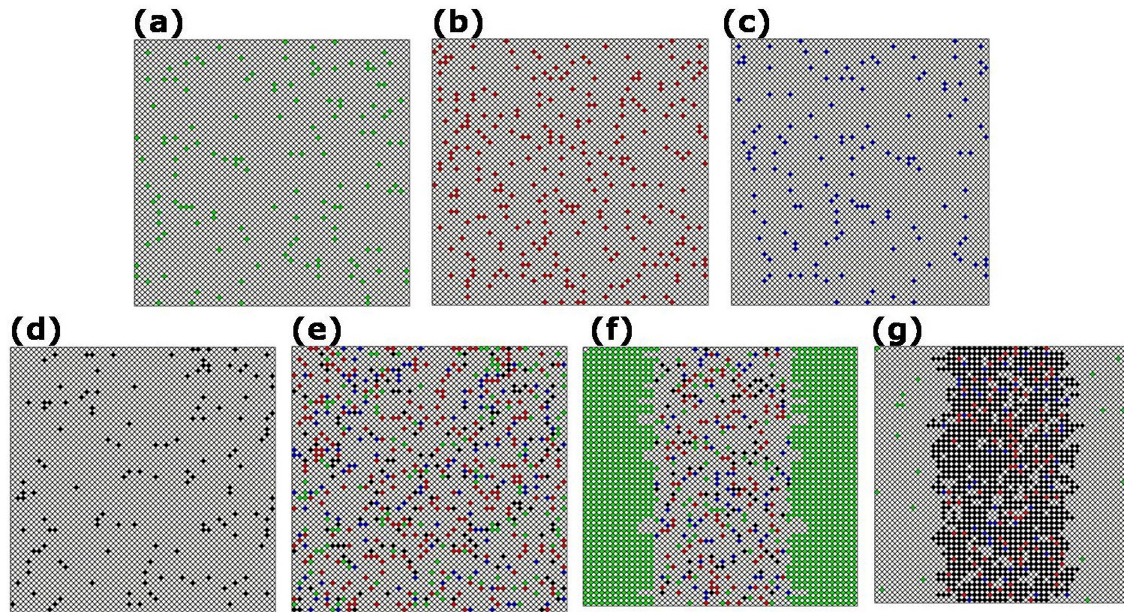

Fig. 1. Monte-Carlo simulation results for a molecular resist: (a) initial acid distribution (5.04%) with a 2-nm diffusion length coefficient, (b) initial PAG distribution before exposure (10.48%), (c) initial quencher distribution (5.4%) with a 2-nm diffusion length coefficient, (d) initial inhibitor distribution (5.4%), (e) initial mixed distribution before exposure, (f) mixed distribution after exposure according to the parameters given in Table 1, and (g) inhibitor distribution after 30 s of PEB in a 2-dimensional plane (100 nm × 100 nm).

a 0.3-μm radius, a 0.8 NA, a 0-μm defocus, and a binary mask with a 60-nm feature size, a 400-nm pitch, and a 280-nm thickness [6]. For Fig. 1(f), the probability $P(x, y, z)$, that a PAG molecule at a position is converted to acid is just equal to the relative fraction of PAG molecules that are converted to acid:

$$P(x, y, z) = [PAG]_{t=0} \left(1 - e^{-CE}\right). \quad (8)$$

Due to the probability, the number of acid molecules is determined. For PEB in Fig. 1(g), the acid latent image due to quencher with a 2-nm DL is created by randomly removing the nearest-neighbor acid-quencher pairs. The deblocking efficiency would be the ratio of the number of inhibitors available to react with acid, which has diffused with a 2-nm DL of acid for a PEB time of 30 s. The line edge is determined by the deblocked gradients along the perpendicular to the mask edge. The RMS (root mean square) roughness is calculated as

$$\sigma_{rms} = \left[\frac{1}{N}\sum_{i=1}^{N}(z_i - Z_{av})^2\right], \quad (9)$$

where z_i is the value at the i-th point and Z_{av} is the mean value. For the convenient calculation, all component sizes are assumed to be the same as the size of a final synthesized component after the lithography process.

For the 45-nm pattern formation, when the mask critical dimension (CD) is larger, a larger exposure dose is required in Fig. 2(a). This effect was the same as that of Fig. 7(a) of Ref. 7. The impact of the acid DC to dose does not show below a 60-nm mask CD, because the effect of dose on the mask CD is larger than that of the acid DC. For the correspondence to the well-known knowledge that the LER has a relation with $(Dose)^{-1/2}$, the LER simulation (●) is an excellent fit of $(aerial\,image\,contrast)^{-1/2}$ in Fig. 2(b). The results shifted down by 3 nm agree well with the experimental results (■) of Pawloski *et al.* [8]. When the image contrast decreases, the transition region with the highest fluctuation in dissolution behavior becomes broader, and the LER is increased. The initial resist conditions of a 60-nm pattern formation in Fig. 2(c) are 10% PAG and 5% quencher, 5% inhibitor, 5% acid, 2-nm quencher DC, and 2-nm acid DC. When the acid DL is larger, LER is smaller. Its effect was the same as that of Fig. 4 of Ref. 9. For the initial resist conditions of a 45-nm pattern formation with 5-nm quencher DC and 5-nm acid DC in Fig. 2(d), increasing the PAG loading until 20% improves LER. This effect was the same as that of Fig. 8(a) of Ref. 7. The decreasing slope of the low dose (■) is sharper than that of the higher dose (●) due to the increased PAG. The initial quencher relative to 30% PAG loading varied between 0 and 0.8 at 40-nm DLs of both acid and quencher in Fig. 2(e). Increasing the quencher loading between 0 and 0.6 ratios of quencher to acid prevents the acid reaction, sharpens the broaden peaks in the de-protected polymer distribution, and leads to a decreased LER. This effect was the same as that of Fig. 6(b) of Ref. 9. The simulated LER values of a 5-nm polymer size (▲) are roughly 10-nm higher than the sim-

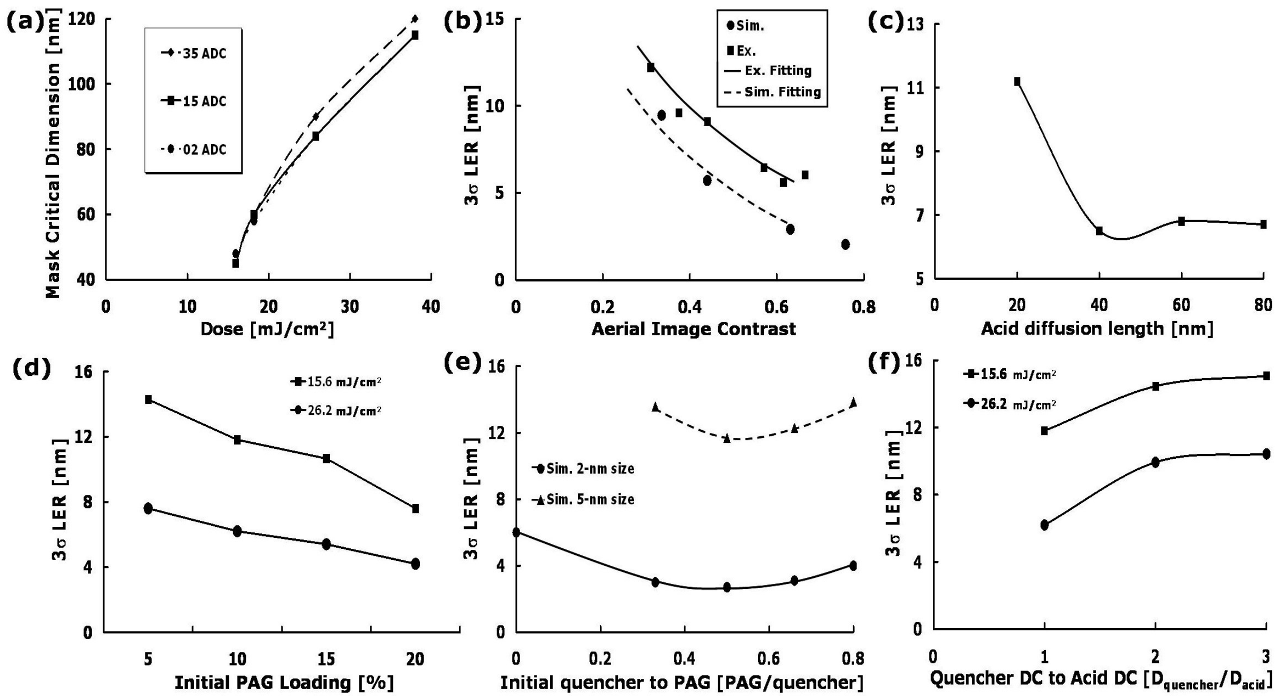

Fig. 2. Impact of (a) dose to Mask CD for the 45-nm pattern formation, (b) aerial image contrast, (c) acid diffusion length, (d) initial PAG loading, (e) initial quencher concentration (PAG/quencher), and (f) quencher diffusion coefficient (Quencher DC / Acid DC) to 3 σ LER. 'ADC' in the graph legend of Fig. 2(a) indicates 'acid diffusion coefficient.' 'Sim. 2-nm size' and 'Sim. 5-nm size' in the graph of Fig. 2(e) indicate 'Simulation in 2-nm polymer size,' and 'Simulation in 5-nm polymer size.'

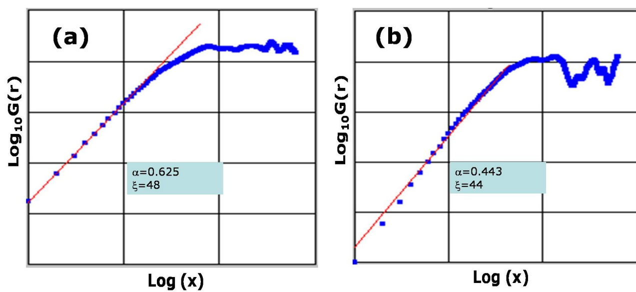

Fig. 3. Height-height-correlation functions (HHCFs) for a 45-nm critical dimension with 26.2 mJ/cm^2 dose due to PAG loadings of (a) 15% and (b) 20%. For the initial 15% PAG, α is 0.625 and ζ is 48, and for the initial 20% PAG, α is 0.443 and ζ is 44.

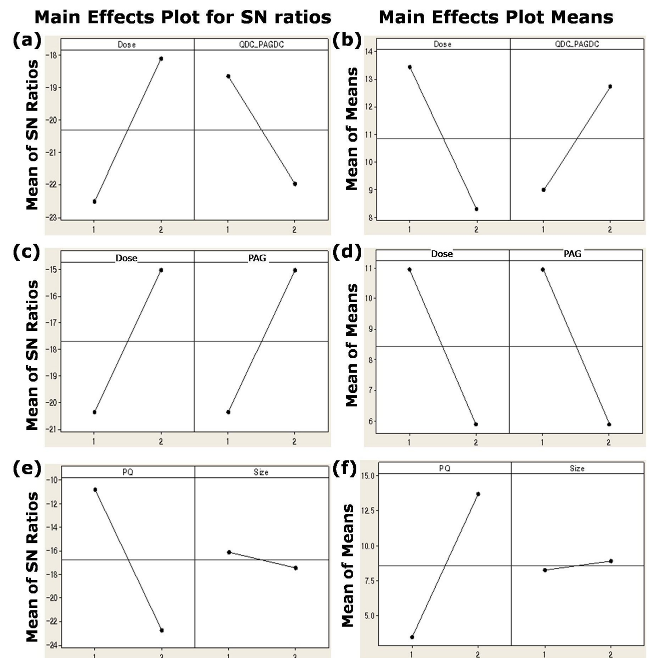

Fig. 4. Main effect plots of S/N ratios and mean. (a) and (b) Dose vs. the ratio of quencher DC to PAG DC. (c) and (d) Dose vs. PAG. (e) and (f) The ratio of PAG to quencher vs. Size.

ulated values of a 2-nm polymer size (•). Hence, when the polymer size is decreased, the LER can be decreased. When the ratio of acid DC to quencher DC is larger than 1, the LER is increased at both low and high doses in Fig. 2(f). This effect was the same as that of Fig. 1(a) of Ref. 10 because the LER corresponds to the slope of the concentration of protected units with distance.

Figure 3 depicts the height-height-correlation function (HHCF) G on a logarithmic axes averaged over all lines included in the image:

Table 1. Simulation parameters along with their levels for the Taguchi method.

	Level 1	Level 2
Dose	15.6	26.2
PAG	5	20
QDC/PAG DC	1	3
PAG/Quanch	0.33	0.8
Size	2-nm	5-nm

Table 2. S/N ratios and means for simulated parameters.

S/N			Mean		
Level	Dose	QCD_PAGDC	Level	Dose	QCD_PAGDC
1	–22.50	–18.65	1	13.44	9.005
2	–18.11	–21.96	2	8.315	12.75
Delta	4.40	3.32	Delta	5.125	3.745
Rank	1	2	Rank	1	2

S/N			Mean		
Level	Dose	PAG	Level	Dose	PAG
1	–20.36	–20.36	1	10.94	10.94
2	–15.04	–15.04	2	5.9	5.9
Delta	5.31	5.31	Delta	5.04	5.04
Rank	1.5	1.5	Rank	1.5	1.5

S/N			Mean		
Level	PQ	Size	Level	PQ	Size
1	–10.76	–16.10	1	3.5	8.29
2	–22.75	–17.44	2	13.72	8.93
Delta	11.95	1.34	Delta	10.22	0.64
Rank	1	2	Rank	1	2

$$G(md) = \left[\frac{1}{N-m} \sum_{i=1}^{N-m} (y_{i+m} - y_i)^2 \right]^{1/2}, \qquad (10)$$

where y_i is the height (distance from a reference axis) of the edge points, N is the number of edge points, m is an integer, and $d = x_{i+1} - x_i$. As HHCF is a quantity of the edge point correlation, it can give information about the spatial aspects of the LER. For a 45-nm CD with a 26.2-mJ/cm^2 dose, the roughness exponent α for the spatial complexity of the roughness and the correction length ζ for the dependence of sigma on the edge length in Fig. 3 are different due to PAG loadings. For the initial 15% PAG, α is 0.625 and ζ is 48, and for the initial 20% PAG, α is 0.443 and ζ is 44.

Table 1 shows the design factors along with their levels for the Taguchi method. The parameters are the resist compositions and the lithography process conditions, which are the most widespread among the researchers to control LER: dose, PAG, the ratio of quencher DC to PAG DC, the ratio of PAG to quencher, and the molecular size.

Since the simulation data can be validated by comparison with experiment data, the reliable data of Fig. 2 are applied to the Taguchi method in Table 2. $L_4(2^2)$ orthogonal arrays, which have 2 rows corresponding to the number of simulations (25 degrees of freedom) with 2 columns at two levels, are chosen for the relations dose vs. the ratio of quencher DC to PAG DC, dose vs. PAG, and the ratio of PAG to quencher vs. molecular size. For S/N ratios by using Eq. (7) and means for the parameters, Table 2 shows the average of the selected characteristic for each level of the factors and ranks then based on Delta statistics, which compare the relative magnitude of effects. Ranks are assigned based on Delta values; rank 1 is assigned to the highest Delta value and rank 2 to the second highest Delta value. Hence, according to Table 2, the effect of PAG on the LER is similar to that of the dose, that of dose is larger than that of the ratio of quencher DC to PAG DC, and that of the ratio of PAG to quencher is larger than that of the molecular size.

Figure 4 shows the corresponding main S/N effect and mean plots between the parameters in Table 2. In the effect plots, if the line of a particular parameter is near horizontal, then the parameter has no significant effect. On the other hand, a parameter for which the line has the highest inclination will have the most significant effect. For its application, the results from the S/N effect and mean plots can clearly describe the results from the ranks of Table 2. A larger S/N in Eq. (7) corresponds to a smaller LER. Hence, the optimal lithography process parameters were Dose of level 2, QDC_PAGDC of level 1, PAG of level 2, PQ of level 1, and Size of level 1, *i.e.* a 26.2-mJ/cm^2 dose, 1 for the ratio of quencher DC to PAG DC, 20% PAG, 0.33 for the ratio of PAG to quencher, and 2-nm for the molecular size. For simulation results, the 13.86-nm LER with the initial parameter settings, which are a 15.6-mJ/cm^2 dose, 10% PAG, 0.8 for the ratio of PAG to quencher, 1 for the ratio of quencher DC to PAG DC, and 5-nm for the molecular size, are optimized to a 3.2-nm LER with the optimal settings.

The molecule-scale simulation is based on the random distribution and the random chemical reaction of each component of the resist. Hence, the random simulation results of specific parameters can be random, so an acceptable range of accuracy and reliability must be found by matching to the experimental results.

V. CONCLUSION

For the ultimate goal to enable prediction of the line-edge-roughness (LER) based upon fundamental and measurable properties of materials, a molecular-scale simulation of resist based on the Monte Carlo method for the master equation is described. Its accuracy and reliability to compare with experimental results is demonstrated. The HHCF (Height-height correction function)

of the spatial scaling metrics for the resist characterization can be used to analyze the LER, because its roughness exponent and correction length are different due to PAG loadings. The Taguchi method can be used to show that the effect of PAG on LER is similar to that of the dose, that of the dose is larger than that of the ratio of quencher DC to PAG DC, and that of the ratio of PAG to quencher is larger than that of the molecular size. The optimal lithography process parameters, which are a 26.2-mJ/cm^2 dose, a 1 ratio of quencher DC to PAG DC, 20% PAG, a 0.33 ratio of PAG to quencher, and a 2-nm size, can reduce a 13.86-nm LER to a 3.2-nm LER in the simulation.

ACKNOWLEDGMENTS

This research was supported by Basic Science Research Program through the National Research Foundation on Korea (NRF) funded by the Ministry of Education, Science and Technology (2009-0074676).

REFERENCES

[1] G. M. Schmid, M. D. Smith, C. A. Mack, V. K. Singh, S. D. Burns and C. G. Willson, Proc. SPIE **4345**, 1037 (2001).
[2] T. Mülders, W. Henke, K. Elian, C. Nölscher and M. Sebald, J. Microlith. Microfab. Microsyst. **4**, 043010 (2005).
[3] S.-K. Kim, J. Korean Phys. Soc. **49**, 1211 (2006).
[4] P. J. Ross, *Taguchi Techniques for Quality Engineering*, 2nd ed. (McGraw-Hill, New York, 1996).
[5] S.-K. Kim, J. Korean Phys. Soc. **50**, 1952 (2007).
[6] S.-K. Kim and H.-K. Oh, J. Korean Phys. Soc. **53**, 3578 (2008).
[7] A. Lawson, C.-T. Lee, W. Yueh, L. Tolbert, C. L. Henderson, Proc. SPIE **6923**, 69230Q (2008).
[8] A. R. Pawloski, A. Acheta, I. Lalovic, B. L. Fontaine and H. J. Levinson, Proc. SPIE **5376**, 414 (2004).
[9] T. Schnattinger and A. Erdmann, Proc. SPIE **6923**, 69230R (2008).
[10] T. Kozawa, S. Tagawa, J. J. Santillan, M. Toriumi and T. Itani, Proc. SPIE **6923**, 69230P (2008).